

# A Useful Approximation for Computing the Continuum Polarization of Be Stars

David McDavid<sup>1</sup>

*Limber Observatory, 135 Star Run, PO Box 63599, Pipe Creek TX 78063*

mcdavid@limber.org

## ABSTRACT

This paper describes a practical model for the polarization of Be stars which can be used to estimate roughly the physical parameters for optically thin circumstellar envelopes from broadband *UBVRI* photopolarimetry data. Analysis of long-term variability in terms of these parameters is a promising approach toward understanding the Be phenomenon. An interesting result from fitting the model to observations of eight Be stars is that all of them may have geometrically thin disks, with opening half-angles on the order of ten degrees or less. This contributes to the growing evidence that most Be disks are geometrically thin.

*Subject headings:* polarization—scattering—techniques:polarimetric—stars: emission-line, Be—stars:winds, outflows—circumstellar matter

## 1. Motivation

The idea that the  $H\alpha$  emission lines of Be stars originate from an equatorially flattened circumstellar envelope or disk has now been directly verified by interferometric imaging (Quirrenbach et al. 1997). The related explanation of the linear polarization of Be stars as due to scattering of the starlight by free electrons in the disk was also confirmed, because the observed position angle of the polarization was found to be perpendicular to the direction of elongation of the disk as projected onto the plane of the sky. It is this apparent asymmetry of the scattering region that results in a net polarization, by defeating the cancellation which would take place if there were identical scattering subregions in adjacent quadrants of the projected disk (see Fig. 1).

A thorough historical review of both observation and theory of polarization in Be stars was given by Coyne & McLean (1982). Since that time the major observational developments in the field have been increased spectral resolution by spectropolarimetry and extension of the wavelength coverage into the ultraviolet by space-based observations (Bjorkman 2000). Beginning with

---

<sup>1</sup>Astronomical Institute, University of Amsterdam, Netherlands

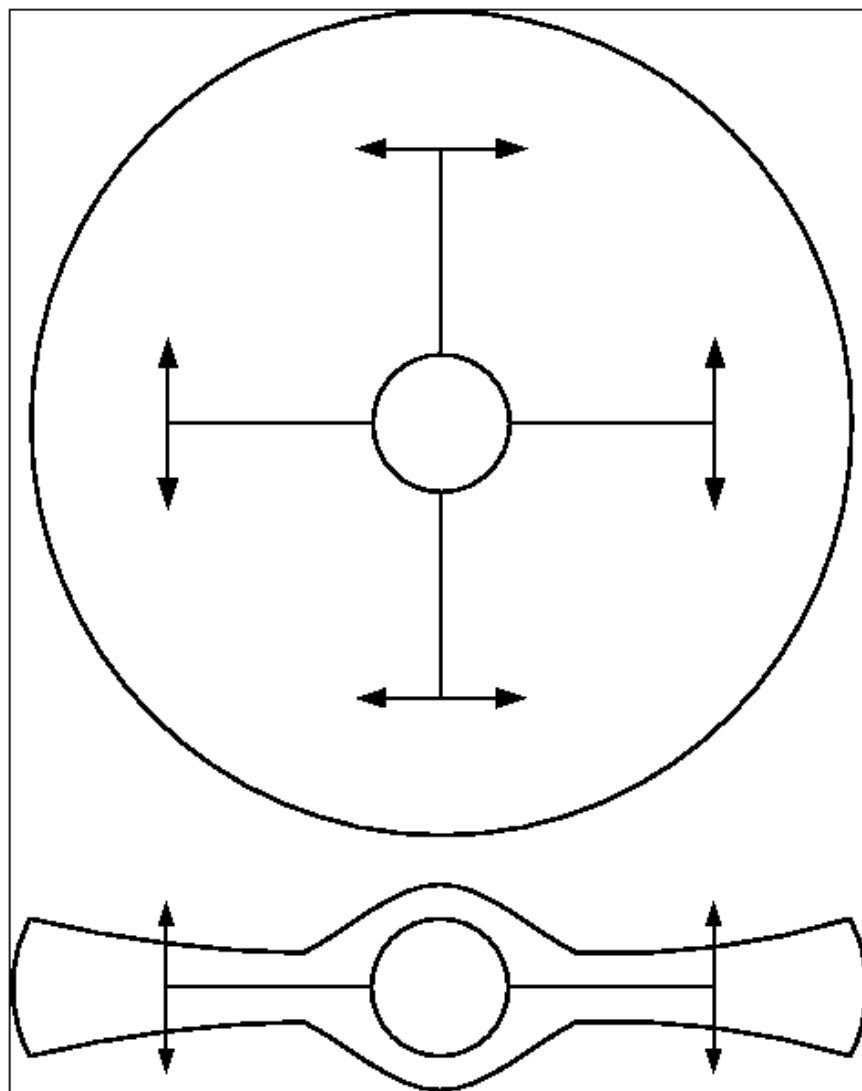


Fig. 1.— Scattering geometry in the disk of a Be star, illustrating by extremes how the net polarization depends on the orientation of the disk on the sky. In the upper sketch the disk is viewed pole-on, with angle of inclination to the line of sight  $i = 0^\circ$ , while in the lower sketch the disk is viewed equator-on, with  $i = 90^\circ$ . Double arrows show the direction of vibration of the electric field of starlight scattered in the disk. For the pole-on case cancellation occurs between adjacent quadrants of the disk, and the net polarization is zero because the electric fields of the scattered light are perpendicular. When the disk is viewed equator-on there is no cancellation, so the observed polarization is a maximum.

the pioneering work of Poekert & Marlborough (1978a,b), who calculated the single scattering polarization in an NLTE hydrogen envelope, theoretical analysis and modeling of the continuum polarization of Be star disks has progressed through increasingly complicated treatments. Fox (1991) developed analytic equations to calculate the single scattering polarization for axisymmetric envelopes. Bjorkman & Bjorkman (1994) extended the single scattering calculations to include attenuation and emission within the envelope. Hillier (1994) developed polarization source functions using traditional Feutrier methods to integrate the transfer equation for optically thick cases, while Wood, Bjorkman, & Bjorkman (1997, hereafter WBB) developed Monte Carlo methods.

One may wonder, then, if there is anything new to be learned about Be stars from continued broadband polarimetry. The answer is, of course, that even though we now have firmer knowledge of the disk characteristics, including temperature, density, and geometry, broadband polarization monitoring is still a primary source of information on the variability of these quantities over time scales of years to decades, which are typical of the most fundamental aspect of the Be phenomenon: the unpredictable transition from the normal B phase to the Be phase and back again, associated with the formation and later dissipation of the circumstellar envelope.

This paper attempts to establish a simple and approximate, but nevertheless serviceable approach to the modeling and analysis of *UBVRI* polarimetry data to derive the basic envelope parameters. Tracing the observed variability in terms of these parameters still promises to give valuable hints about the nature of the unknown processes involved in the Be phenomenon.

## 2. A Spherical Sector Envelope Model

Figure 2 shows the geometry of the circumstellar envelope model adopted for this study. Introduced by Kruszewski, Gehrels, & Serkowski (1968) to investigate the polarization of red variables, it was later used by Brown & McLean (1977) to illustrate their theoretical formulation of the polarization by electron scattering in a Be disk. Its shape may be described as an axially symmetrical sector of a sphere, with a wedge-shaped cross section opening outward at half-angle  $\alpha$ .

For small opening angles the spherical sector is a good representation of an equatorial disk, with the advantage of being mathematically suited for spherical coordinates. A basic starting point is to assume the disk is pure hydrogen with uniform electron temperature  $T_e$ , extending to infinite distance ( $R_e \rightarrow \infty$  in Fig. 2) from a central star of radius  $R_*$ , with electron number density  $N_e$  given by a radial power law with exponent  $\eta$ :

$$N_e(r) = N_{0e} \left( \frac{R_*}{r} \right)^\eta . \quad (1)$$

Waters, Coté, & Lamers (1987) derived values of  $2.0 < \eta < 3.5$  for some of the stars also studied in this paper using the slope of the infrared continuum from *IRAS* observations, but the

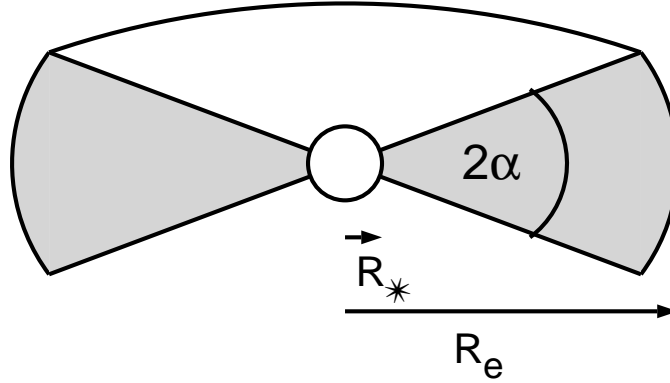


Fig. 2.— Cutaway view of the spherical sector model adopted for the circumstellar envelope.

spherical sector model with  $R_e \rightarrow \infty$  has the peculiarity that the disk mass is infinite unless  $\eta > 3.0$ . In what follows, the symbol  $\eta$  will be retained for generality, but  $\eta = 3.1$  is used as a representative mean value in all the numerical computations.

### 3. An Approximation for the Gray Polarization

According to Fox (1991) except for a sign error in the first argument of the beta function  $B$ , the net polarization of light from a central star due to scattering of photons by free electrons (Thomson scattering) in a surrounding envelope may be roughly approximated for the specific case of the infinite spherical sector geometry as

$$p_0 = \frac{3(\eta - 1)}{16} B\left(\frac{\eta - 1}{2}, \frac{3}{2}\right) \tau_e \sin \alpha \cos^2 \alpha \sin^2 i, \quad (2)$$

where  $i$  is the angle of inclination of the rotation axis of the star to the line of sight and

$$\begin{aligned} \tau_e &= \int_{R_*}^{\infty} N_{0e} \left(\frac{R_*}{r}\right)^\eta \sigma_e dr \\ &= \frac{N_{0e} \sigma_e R_*}{\eta - 1} \text{ (finite only for } \eta > 1.0) \end{aligned} \quad (3)$$

is the total radial optical depth for electron scattering in the equatorial plane of the spherical sector in terms of the Thomson scattering cross section

$$\sigma_e = \frac{8\pi}{3} \left(\frac{e^2}{mc^2}\right)^2. \quad (4)$$

Equation (2) is only a single-scattering approximation, based on the assumption that the disk is optically thin and neglecting multiple scattering. It includes a correction for the geometrical complication that the star is an extended source of light and cannot be treated as a point source (Cassinelli, Nordsieck, & Murison 1987, hereafter CNM), but it does not take into account the occultation of part of the scattering envelope by the star.

#### 4. Including the Wavelength Dependence

So far the calculated polarization has no dependence on wavelength, since it comes from pure electron scattering. However, neutral hydrogen in the envelope absorbs some light both before and after scattering, and the envelope emission (which is treated here as unpolarized and is not considered to scatter) dilutes the polarization. It is therefore necessary to include these wavelength-dependent effects, since they combine to produce the slope of the continuum polarization and the well-known abrupt changes in the polarization at the HI ionization series limits, as first demonstrated by Capps, Coyne, & Dyck (1973) and later refined by McLean (1979).

Assuming LTE ionization fractions and level populations, equation (5) gives the total wavelength-dependent opacity  $\kappa(\lambda)$  per gram of neutral hydrogen in the ground state (Aller 1963).  $C_0$  is a fixed numerical factor,  $X(n)$  is the ionization energy from level  $n$  in units of  $kT_e$ , and  $C_{se}$  is the correction factor for stimulated emission. The three individual terms in the equation are a summation over the ionization edges of the first seven discrete energy levels, an integrated term for the combination of all the remaining levels, and a free-free absorption term (with Gaunt factors taken to be unity). See Appendix A for a discussion of NLTE corrections.

$$\kappa(\lambda) = C_0 e^{-X(1)} \lambda^3 \left( \sum_{\lambda < \lambda_n}^{X(n)} \frac{e^{X(n)}}{n^3} + \frac{(e^{X(8)} - 1)}{2X(1)} + \frac{1}{2X(1)} \right) C_{se}, \quad (5)$$

where

$$C_0 = \frac{32\pi^2 e^6 R}{3\sqrt{3} m_H h^3 c^3}, \quad (6)$$

$$X(n) = \frac{2\pi^2 m_e e^4}{n^2 h^2 k T_e}, \quad (7)$$

and

$$C_{se} = \left( 1 - e^{-hc/\lambda k T_e} \right). \quad (8)$$

If the free electron number density  $N_e(r)$  and the electron temperature  $T_e$  are known, then the number density  $N_1(r)$  of neutral hydrogen atoms in the ground state can be found from the Saha equation:

$$\begin{aligned} N_1(r) &= \frac{h^3}{(2\pi m_e k T_e)^{3/2}} N_e^2(r) e^{X(1)} \\ &= N_{01} \left( \frac{R_*}{r} \right)^{2\eta}, \end{aligned} \quad (9)$$

where

$$N_{01} = \frac{h^3}{(2\pi m_e k T_e)^{3/2}} N_{0e}^2 e^{X(1)}. \quad (10)$$

The total radial optical depth for neutral hydrogen absorption in the equatorial plane of the spherical sector is therefore

$$\begin{aligned} \tau_a(\lambda) &= \int_{R_*}^{\infty} \kappa(\lambda) m_H N_{01} \left( \frac{R_*}{r} \right)^{2\eta} dr \\ &= \frac{N_{01} m_H \kappa(\lambda) R_*}{2\eta - 1} \text{ (finite only for } \eta > 0.5), \end{aligned} \quad (11)$$

which acts as a wavelength-dependent attenuation factor to reduce the gray polarization.

The volume emission coefficient of the envelope is

$$j(\lambda, r) = m_H \kappa(\lambda) N_{01} \left( \frac{R_*}{r} \right)^{2\eta} B(\lambda), \quad (12)$$

where

$$B(\lambda) = \frac{2hc^2}{\lambda^5 (e^{hc/\lambda k T_e} - 1)} \quad (13)$$

is the Planck function (not to be confused with the beta function in §3). The total luminosity of the envelope is then

$$\begin{aligned} L(\lambda) &= 4\pi \int_0^{2\pi} \int_{\frac{\pi}{2}-\alpha}^{\frac{\pi}{2}+\alpha} \int_{R_*}^{\infty} j(\lambda, r) r^2 \sin \theta dr d\theta d\phi \\ &= \frac{16\pi^2}{2\eta - 3} N_{01} m_H \kappa(\lambda) B(\lambda) R_*^3 \sin \alpha \text{ (finite only for } \eta > 1.5), \end{aligned} \quad (14)$$

which together with the stellar flux  $F_*(\lambda)$  produces a further wavelength dependence of the polarization. Theoretical values of the stellar flux  $F_*(\lambda)$  are taken from tabulated model atmospheres by Kurucz (1994).

With the wavelength dependence included, our polarization estimate may now be written as

$$p(\lambda) = \frac{p_0 e^{-\tau_a(\lambda)}}{1 + L(\lambda)/(4\pi R_*^2 F_*(\lambda))}. \quad (15)$$

It should be emphasized that this equation is only an approximation (even if the disk is optically thin), since it includes neither the contribution of scattering of the disk emission to the polarization nor attenuation of the direct starlight by the disk. Also the neutral hydrogen opacity is treated in a very crude way, using only the maximum radial optical depth in the equatorial plane.

It may be of interest to calculate the total mass of the disk, which can be done approximately by simply counting pairs of electrons and protons under the assumption that it consists purely of fully ionized hydrogen:

$$\begin{aligned} M &= \int_0^{2\pi} \int_{\frac{\pi}{2}-\alpha}^{\frac{\pi}{2}+\alpha} \int_{R_*}^{\infty} m_H N_{0e} \left(\frac{R_*}{r}\right)^\eta r^2 \sin\theta dr d\theta d\phi \\ &= \frac{4\pi}{\eta-3} N_{0e} m_H R_*^3 \sin\alpha \quad (\text{finite only for } \eta > 3.0). \end{aligned} \quad (16)$$

## 5. Synthesizing Broadband Data

Adjustment of the envelope parameters in the theoretical model to give results consistent with observations might be expected to yield valuable information about the nature of Be disks. To compare with observations on the Johnson-Cousins *UBVRI* system, it is first necessary to convolve the theoretically estimated polarization  $p(\lambda)$  from equation (15) with the bandpass characteristics of the optical system.

As a first approximation, let us assume Gaussian filter transmission curves based on the standard *UBVRI* wavelengths and *fwhm* (Bessell 1979), which are closely matched by the system actually used for the observations (see Table 1).

Given the central wavelength  $\lambda_c$ , the standard deviation  $\sigma$  can be calculated from the *fwhm*  $\Gamma$  since  $\Gamma = 2.354 \sigma$  for a Gaussian distribution, so that the transmission function may be written as

$$T(\lambda) = \exp \left[ -\frac{1}{2} \left( \frac{\lambda - \lambda_c}{\Gamma/2.354} \right)^2 \right]. \quad (17)$$

The theoretical total flux  $F(\lambda)$  is due to the stellar component  $F_*(\lambda)$  plus the envelope component:

$$F(\lambda) = F_*(\lambda) + L(\lambda)/(4\pi R_*^2). \quad (18)$$

Convolving the polarization in terms of flux with the transmission function, where  $\lambda_{min}$  and  $\lambda_{max}$  are, to a realistic approximation, the 10% response points, we find a theoretical expression for the expected polarization over the given bandpass:

$$P(BP) = \frac{\sum_{\lambda=\lambda_{min}}^{\lambda_{max}} p(\lambda)F(\lambda)T(\lambda)\Delta\lambda}{\sum_{\lambda=\lambda_{min}}^{\lambda_{max}} F(\lambda)T(\lambda)\Delta\lambda}. \quad (19)$$

## 6. Adjustable Parameters & Model Fits

With the model in hand, an interactive graphical computer interface was designed to allow adjusting the input parameters by trial and error to fit *UBVRI* polarization measurements (McDavid 1999) of eight Be stars. Solutions obtained this way should be viewed with some caution since they may not be unique: different geometrical distributions of scatterers can produce the same net polarization. Moreover, given the gross approximations involved, only order-of-magnitude results should be expected.

The model disk has three adjustable parameters: the maximum electron number density  $N_{0e}$ , the angle of inclination  $i$  of the rotation axis to the line of sight, and the opening half-angle  $\alpha$ . Additionally required fixed parameters for each individual star are the radius  $R_*$ , the effective temperature  $T_*$ , and the surface gravity  $\log g$ , which were estimated from Table 1 of Collins, Truax, & Cranmer (1991) based on spectral types from Slettebak (1982). The electron temperature of the disk was then fixed at  $T_e = 0.75 T_*$  and the appropriate Kurucz flux table chosen to match  $T_*$  and

Table 1. Filter System Parameters

Filter	Effective Wavelength (Å)	Bandpass ( <i>fwhm</i> ) (Å)
<i>U</i>	3650	700
<i>B</i>	4400	1000
<i>V</i>	5500	900
<i>R</i>	6400	1500
<i>I</i>	7900	1500

$\log g$ .

The fixed disk temperature  $T_e$  affects the wavelength dependence of the polarization through its influence on the neutral hydrogen opacity by setting the degree of ionization and the populations of the excited states (eq. [5]). It influences not only the hydrogen absorption optical depth (eq. [11]), but also the disk luminosity (eq. [14]), which is another contributor to the wavelength dependence of the polarization. As a result,  $T_e$  is important in determining the polarization Balmer jump and the slope of the polarization over the Paschen continuum, both of which generally increase at lower temperatures. Appendix A explains the NLTE corrections to the level populations which are necessary to fit these features for some of the program stars.

It is instructive to summarize individually the effects of the three adjustable parameters on the behavior of  $p(\lambda)$  according to equation (15).

(1) The overall degree of gray polarization is directly proportional to  $N_{e0}$  through the factor  $\tau_e$  in equation (2). However, simply increasing  $N_{e0}$  does not always result in an overall polarization increase, because it also increases the attenuation and adds to the wavelength dependence of the polarization through  $\tau_a(\lambda)$  (eq. [11]) and  $L(\lambda)$  (eq. [14]).

(2) The earliest basic electron scattering models (e.g. Brown & McLean 1977) gave a  $\sin^2 i$  dependence of the polarization on  $i$ , and further refinements have not qualitatively changed the simple picture of Figure 1 in which a face-on disk shows no net polarization because of symmetrical cancellation, while the maximum asymmetry of an edge-on disk results in the maximum polarization. It may seem likely that  $i$  is poorly determined in this model since the same polarization might be obtained, for example, by decreasing  $i$  while increasing  $\alpha$ , keeping  $N_{e0}$  constant. Experiments do not bear this out, though, because a thicker disk has a higher luminosity, which changes the wavelength dependence of the polarization enough to ruin the fit (eq. [15]). Another helpful constraint on  $i$  is the presence or absence of shell lines, which are thought to be absorption features in the spectral line profiles due to circumstellar material in the line of sight for nearly edge-on equatorial disks. Since Be stars are generally rapid rotators, spectroscopic measurement of the projected rotational velocity  $v \sin i$  can also suggest roughly the value of  $i$ .

(3) Figure 3 shows how the model polarization  $p^B$  in the  $B$  passband varies as  $\alpha$  increases from  $0^\circ$  to  $90^\circ$  using a typical set of parameters. The polarization first rises as the widening disk presents an increasing number of scatterers, then begins to decline due to the buildup of enough density at high latitudes to cancel the polarization from the equatorial regions. The model of Waters & Marlborough (1992) also shows this behavior, which becomes of practical concern because the hump-shaped graph allows for both a “thick disk” and a “thin disk” solution, producing identical polarization at  $\alpha$  values on opposite sides of the peak. For equal densities, however, the thick disk will have a higher luminosity than the thin disk, giving the polarization a recognizably different wavelength dependence.

Figures 4–11 present possible (but not necessarily unique) model fits for the eight program Be stars, with the parameters summarized in Table 2. The observational data points, plotted as open

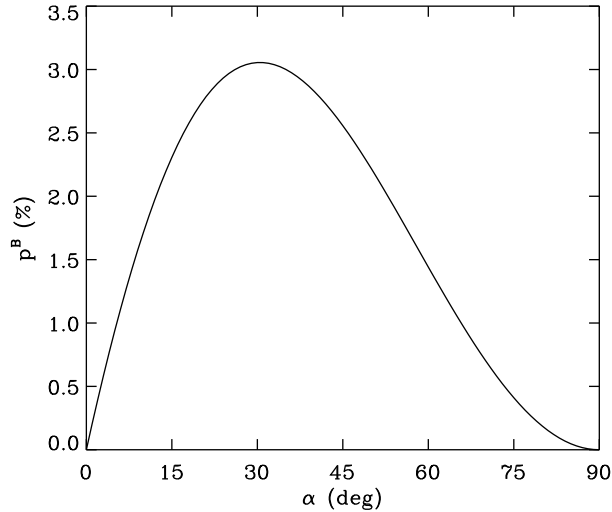


Fig. 3.— The dependence of the model blue polarization  $p^B$  on the opening half-angle  $\alpha$  of the disk using a typical set of parameters.

squares with vertical error bars, are intrinsic polarization, corrected for the interstellar component by Stokes vector subtraction (McDavid 1999). The corresponding model result is plotted as a solid line, using open circles for the broadband values with horizontal line segments to show the filter passbands. Several additional quantities derived from the model are also included in Table 2 for each fit: the maximum polarization  $p_{max}$  and its wavelength  $\lambda(p_{max})$ , the maximum of the H I absorption optical depth  $\tau_{a_{max}}$  and its wavelength  $\lambda(\tau_{a_{max}})$ , the electron scattering optical depth  $\tau_e$ , the total envelope mass  $M$ , and the NLTE departure coefficients  $b_2$  and  $b_3$  for the populations of the first two excited states of the neutral hydrogen in the disk. Refer to Appendix A for a discussion of NLTE considerations.

## 7. Test of Accuracy

Since the model presented here is such a crude approximation, it is important to compare its results with those from a more sophisticated model to investigate, at least qualitatively, the accuracy we can expect. The Monte Carlo code of WBB is one such standard, and it is based on the same set of input parameters except that the density input is the electron scattering optical depth rather than the electron number density, which requires only a minor conversion. Ideally we would like to determine WBB fits to the program star observations, and then quantitatively evaluate the simplified model by direct comparison of the fit parameters. Unfortunately, because of the slow convergence of the Monte Carlo method, deriving a WBB fit is a complex process requiring substantial amounts of cpu time even on a fast computer. Otherwise there would be no reason for interest in the kind of quick approximation that is the subject of this paper.

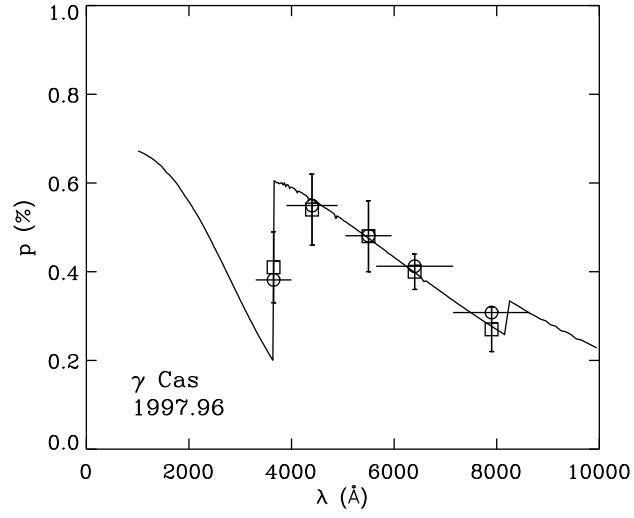


Fig. 4.— Fit of a spherical sector disk to the *UBVRI* polarization of  $\gamma$  Cas.

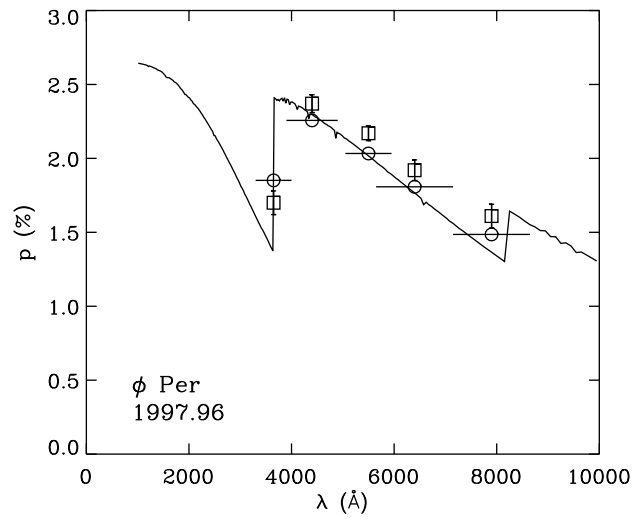


Fig. 5.— Fit of a spherical sector disk to the *UBVRI* polarization of  $\phi$  Per.

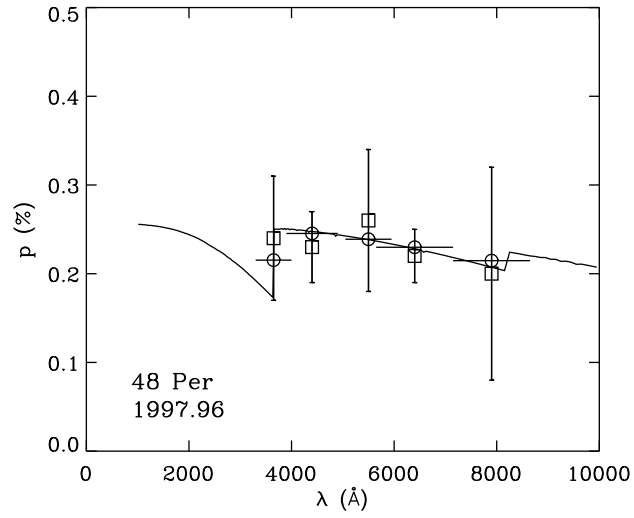


Fig. 6.— Fit of a spherical sector disk to the *UBVRI* polarization of 48 Per.

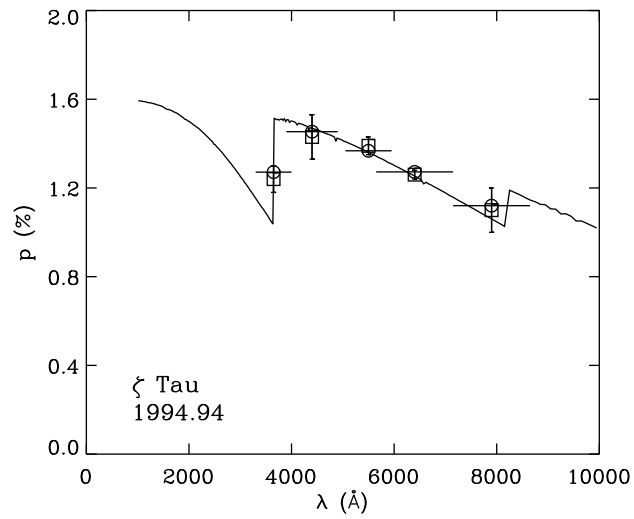


Fig. 7.— Fit of a spherical sector disk to the *UBVRI* polarization of  $\zeta$  Tau.

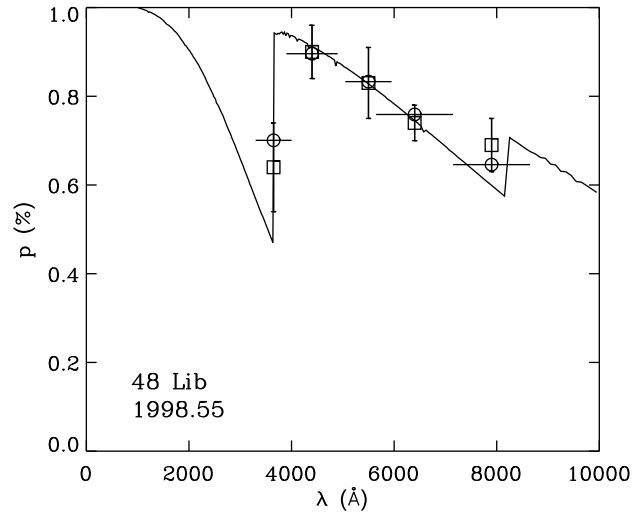


Fig. 8.— Fit of a spherical sector disk to the *UBVRI* polarization of 48 Lib.

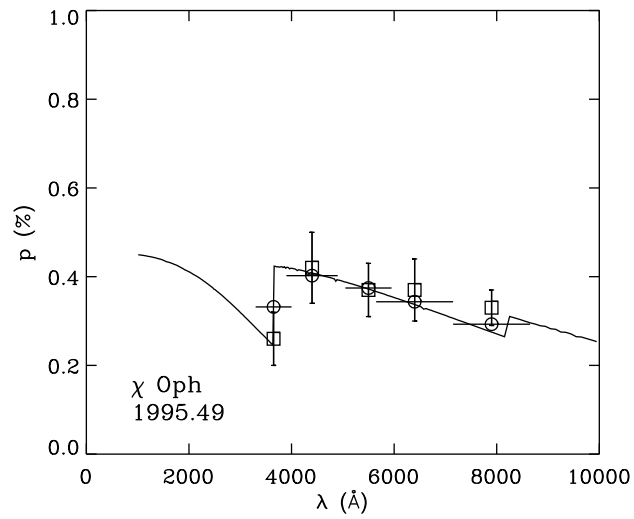


Fig. 9.— Fit of a spherical sector disk to the *UBVRI* polarization of  $\chi$  Oph.

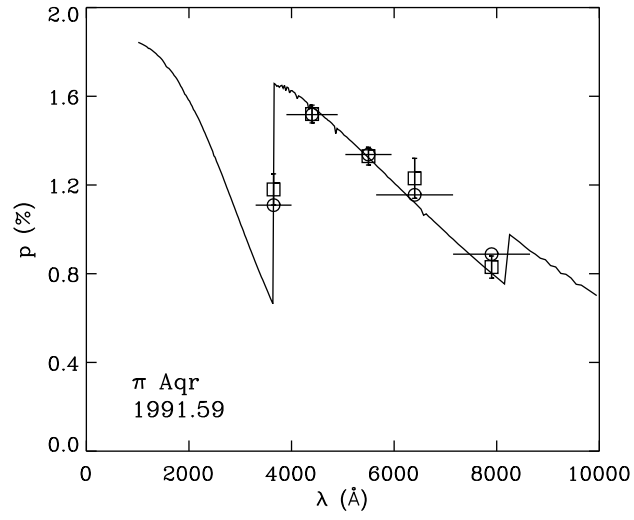


Fig. 10.— Fit of a spherical sector disk to the *UBVRI* polarization of  $\pi$  Aqr.

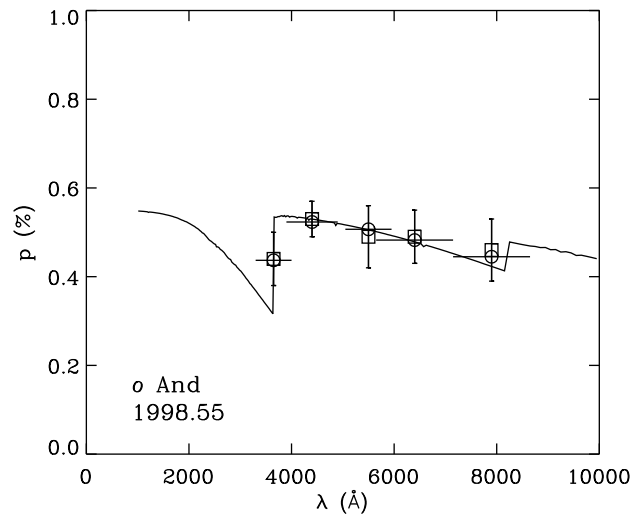


Fig. 11.— Fit of a spherical sector disk to the *UBVRI* polarization of o And.

Table 2. Be Star Modeling Data

	$\gamma$ Cas	$\phi$ Per	48 Per	$\zeta$ Tau	48 Lib	$\chi$ Oph	$\pi$ Aqr	o And
Spectral Type	B0.5 IVe	B1.5 (V:)e-shell	B4 Ve	B1 IVe-shell	B3:IV:e-shell	B1.5 Ve	B1 III-IVe	B6 III
Date of Obs.	1997.96	1997.96	1997.96	1994.94	1998.55	1995.49	1991.59	1998.55
$R_*(R_\odot)$	6.5	6.0	4.5	7.0	6.0	6.0	9.0	5.5
$T_*$ (K)	25,000	25,000	17,000	25,000	20,000	25,000	25,000	14,000
$\log g$	4.0	4.0	4.0	4.0	3.5	4.0	3.5	3.5
$N_{0e}(10^{12}\text{cm}^{-3})$	9.00	5.00	3.00	4.20	4.60	6.20	6.50	2.00
$T_e$ (K)	18,750	18,750	12,750	18,750	15,000	18,750	18,750	10,500
$\alpha$ (deg)	2.0	10.0	3.0	6.0	4.0	3.0	3.5	5.5
$i$ (deg)	52.0	80.0	55.0	80.0	80.0	41.0	80.0	80.0
$pmax$ (%)	0.60	2.41	0.25	1.51	0.94	0.42	1.66	0.54
$\lambda(pmax)$ (Å)	3661	3862	3862	3661	3812	3661	3661	3862
$\tau_{amax}$	0.94	0.27	0.23	0.22	0.44	0.41	0.68	0.22
$\lambda(\tau_{amax})$ (Å)	3636	3636	3636	3636	3636	3636	3636	3636
$\tau_e$	1.29	0.66	0.30	0.65	0.61	0.82	1.29	0.24
$M(10^{-9}M_\odot)$	3.07	6.69	0.51	5.37	2.47	2.50	10.3	1.14
$b_2$	1.69	1.69	1.05	1.69	1.35	1.69	1.69	0.70
$b_3$	0.29	0.29	0.23	0.29	0.26	0.29	0.29	0.19

For the time being, though, we can at least make use of the existing WBB fit to  $\zeta$  Tau. Figure 12 shows examples of  $p(\lambda)$  for the quick approximation (solid line with broadband filter points marked by open circles) compared to the full optically thick multiple scattering WBB simulation (dashed line connecting filled circles). Errors in the WBB data points are on the order of 0.03%, limited by computing time. The observed *UBVRI* data are plotted as open squares with error bars. Using the parameters  $R_* = 5.5 R_\odot$ ,  $T_* = 19,000$  K,  $T_e = 15,000$  K,  $\alpha = 2^\circ.5$ , and  $i = 82^\circ.0$  from the WBB solution as input to both models, the six plots show what happens as  $\tau_e$  is increased by steps from 0.10 to 3.00 (the best fit value according to WBB).

This test shows that the optically thin approximation agrees quite well with the WBB calculation up to and including an optical depth of 1.00. It is also encouraging that for  $\zeta$  Tau the best fit of the approximate method as shown in Figure 7 and Table 2 has  $N_{e0} = 4.20 \times 10^{12} \text{ cm}^{-3}$ , which is well within the range of  $2.38 \times 10^{12} \leq N_{0e} \leq 7.54 \times 10^{12} \text{ cm}^{-3}$  found by Waters, Coté, & Lamers (1987) in their infrared study.

However, it must be noted that there is a possibly serious disagreement between the WBB model and the simplified model presented here with regard to the best-fit values of  $\tau_e$  and  $\alpha$  for  $\zeta$  Tau. While the WBB disk ( $\tau_e = 3.00$  and  $\alpha = 2^\circ.5$ ) is optically thick but geometrically thin, the simplified model disk ( $\tau_e = 0.65$  and  $\alpha = 6^\circ.0$ ) is optically thin and geometrically thicker (although it still qualifies as “geometrically thin”).

In Figure 12 the approximate model fails to produce a polarization large enough to fit the observations of  $\zeta$  Tau by increasing  $\tau_e$  at constant  $\alpha$  because it becomes dominated by H I opacity. As shown in Table 2, this problem is seemingly avoided by increasing  $\alpha$  instead of  $\tau_e$ , but the resulting optically thin solution could possibly be ruled out on other grounds, such as the associated infrared emission as discussed by WBB. This is only one cautionary example emphasizing the importance of independent observational consistency checks in the interpretation of Be-star polarimetry data.

## 8. Conclusion

In summary, the model presented here appears to give reasonable results for optically thin cases, but we should only trust it for order-of-magnitude accuracy because it is based on so many simplifying assumptions. Even so, it may be useful for estimating trial values of the parameters as starting points for rigorous fitting with more elaborate models.

An interesting result from applying the model to observations of the eight program stars is that all of them may be fit with geometrically thin disks, with opening half-angles of ten degrees or less. This adds tentative support to the statistics in favor of thin disks as presented by Bjorkman & Cassinelli (1990) and later discussed at length by WBB. If most Be disks prove to be similarly flat, it will surely have important implications concerning their formation process.

It may seem discouraging that this model will never find optically thick solutions even if they

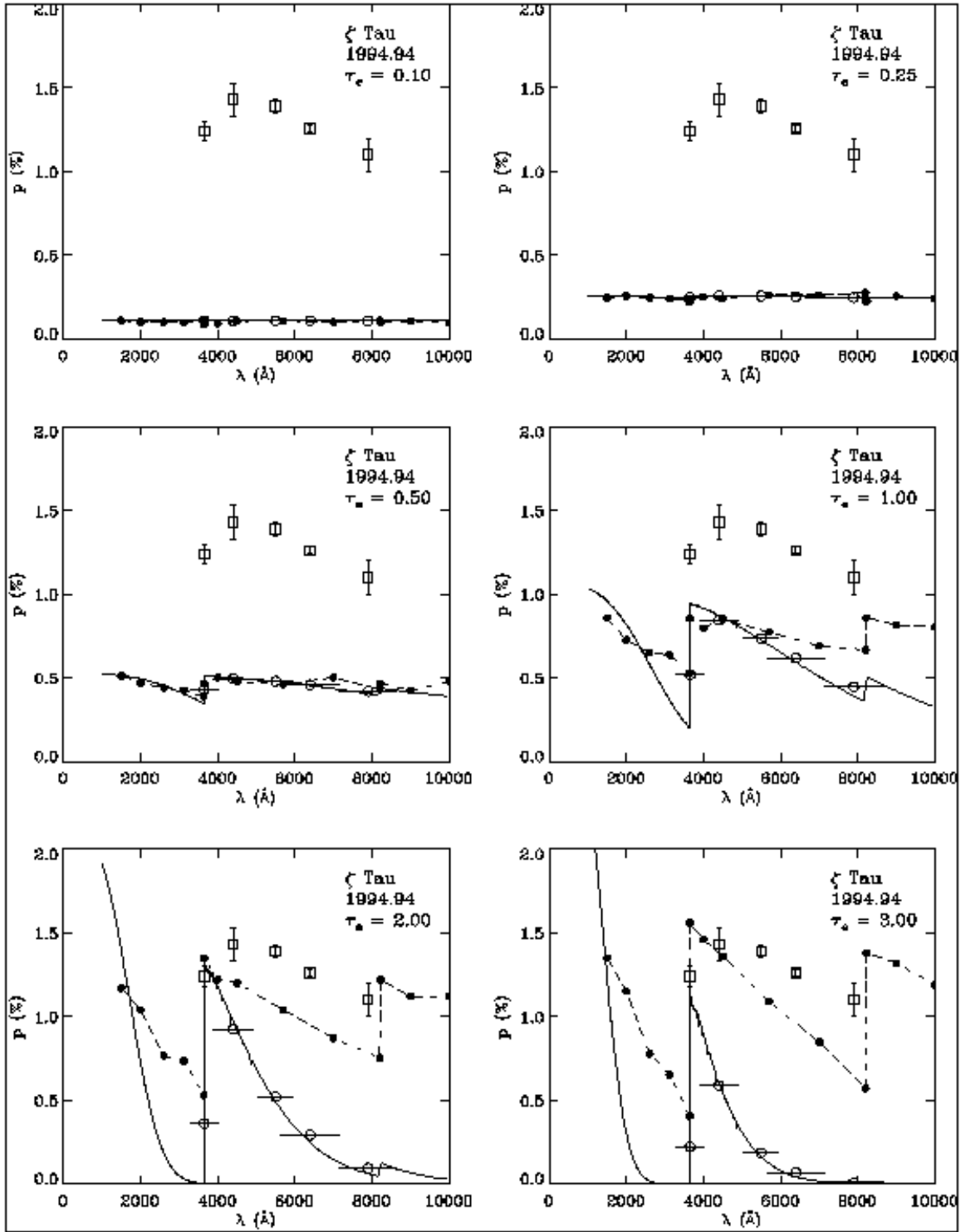


Fig. 12.— A comparison of the simple approximation (solid line with open circles) against the WBB solution (dashed line with filled circles) for a range of electron scattering optical depths  $\tau_e$ . The observational data points for  $\zeta$  Tau are shown as open squares.

physically exist. And with three adjustable parameters, there might be any number of apparently valid optically thin fits to a set of *UBVRI* data points, rendering the entire exercise inconclusive. Nevertheless, there are good reasons for a more optimistic point of view. Due to the efforts of many investigators, as documented, for example, in the references in §1 of this paper, the range of physically allowable parameters has been narrowed significantly. And within even the most liberal of these constraints, experience with a quick, interactive trial-and-error system based on even the elementary physics presented here will show that it is surprisingly difficult to find multiple solutions with qualitatively different sets of parameters. I will be glad to share my IDL modeling program with interested users on request.

Thanks to Joe Cassinelli for critical reading and commentary on early drafts of this paper, and especially for suggesting a method to estimate the NLTE departure coefficients for the neutral hydrogen in a Be disk. Kenny Wood and Barbara Whitney also provided very helpful discussions, and Jon Bjorkman kindly gave me a version of the Monte Carlo polarization code. I especially thank the anonymous referee for pointing out many serious errors in the original manuscript and for patiently explaining the necessary corrections.

### A. Estimating the NLTE Departure Coefficients

Fits to the polarization Balmer jump were difficult and in some cases impossible without NLTE corrections to the level populations of the first two excited states of H I. According to the combined Saha and Boltzmann equations, the maximum population of the first excited state normally occurs at a temperature of about 10,000 K and declines rapidly toward higher temperatures with increasing excitation and ionization. At temperatures closer to 20,000 K appropriate for Be disks, the LTE value of the absorption coefficient at the *U*-band is sometimes too small to match the large polarization Balmer jumps which are commonly observed. NLTE correction is applied only to the first two excited states because they dominate the opacity at optical wavelengths for the conditions of density and temperature of interest.

Since only averages over a line of sight are required for this very approximate polarization model, departure coefficients were simply estimated from the calculations of CNM. Their Figure 3 shows mean population parameters  $\bar{q}_n$  for  $n = 2$  and  $n = 3$  defined by

$$\begin{aligned} \bar{q}_{nNLTE} &\equiv \frac{\int_{R_*}^{\infty} q_n(r, T_*) N_e^2 dr}{\int_{R_*}^{\infty} N_e^2 dr} \\ &= \frac{\int_{R_*}^{\infty} N_n dr}{\int_{R_*}^{\infty} N_e^2 dr}, \end{aligned} \tag{A1}$$

based on the detailed NLTE analysis of a stellar wind immersed in the radiation field of a central

star, with statistical balance between photoionization and radiative recombination. The departure coefficient for level  $n$  is then the ratio of the NLTE and LTE values of  $\bar{q}_n$ .

The calculation of  $\bar{q}_{nLTE}$  is done as follows:

$$\begin{aligned} \int_{R_*}^{\infty} N_n(r) dr &= n^2 N_{01} e^{X(n)-X(1)} \int_{R_*}^{\infty} \left( \frac{R_*}{r} \right)^{2\eta} dr \\ &= \frac{n^2 N_{01} R_*}{2\eta - 1} e^{X(n)-X(1)} \end{aligned} \quad (\text{A2})$$

and

$$\begin{aligned} \int_{R_*}^{\infty} N_e^2 dr &= N_{0e}^2 \int_{R_*}^{\infty} \left( \frac{R_*}{r} \right)^{2\eta} dr \\ &= \frac{N_{0e}^2 R_*}{2\eta - 1}, \end{aligned} \quad (\text{A3})$$

so that

$$\begin{aligned} \bar{q}_{nLTE} &= \frac{\int_{R_*}^{\infty} N_n dr}{\int_{R_*}^{\infty} N_e^2 dr} \\ &= \frac{N_{01}}{N_{0e}^2} n^2 e^{X(n)-X(1)} \\ &= (2\pi m_e k T_e)^{-1.5} h^3 n^2 e^{X(n)}. \end{aligned} \quad (\text{A4})$$

The population parameters  $\bar{q}_{2NLTE}$  and  $\bar{q}_{3NLTE}$  may be estimated by extrapolation of power law fits to the disk temperatures (10,000–20,000 K) and mass-loss rates ( $\sim 10^{-8} M_{\odot} \text{ yr}^{-1}$ ) characteristic of Be stars, based on Figure 3 of CNM:

$$\bar{q}_{2NLTE} = 1.11 \times 10^{-8} T_e^{-2.83}, \quad (\text{A5})$$

$$\bar{q}_{3NLTE} = 4.59 \times 10^{-13} T_e^{-2.02}. \quad (\text{A6})$$

The approximate departure coefficients are then  $b_2 = \bar{q}_{2NLTE}/\bar{q}_{2LTE}$  and  $b_3 = \bar{q}_{3NLTE}/\bar{q}_{3LTE}$ , so that the corrected level populations are roughly  $N_{2NLTE} = b_2 \times N_{2LTE}$  and  $N_{3NLTE} = b_3 \times N_{3LTE}$ . These correction factors are applied to the appropriate terms in the summation inside the parentheses in equation (5). The corrected form of  $\kappa(\lambda)$  is used only in calculating the absorption optical depth and not in calculating the emission coefficient, since recombination and free-free emission are LTE processes.

## REFERENCES

- Aller, L.H. 1963, *The Atmospheres of the Sun and Stars* (New York: Ronald Press)
- Bessell, M.S. 1979, *PASP*, 91, 589
- Bjorkman, J.E. & Bjorkman, K.S. 1994, *ApJ*, 436, 818
- Bjorkman, J.E. & Cassinelli, J.P. 1990, in *Angular Momentum and Mass Loss from Hot Stars*, ed. L.A. Willson & R. Stalio (Dordrecht: Kluwer), 185
- Bjorkman, K.S. 2000, in *IAU Coll. 175: The Be Phenomenon in Early-Type Stars*, ed. M. Smith, H. Henrichs, & J. Fabregat (San Francisco: ASP), 384
- Brown, J.C. & McLean, I.S. 1977, *A&A*, 57, 141
- Capps, R.W., Coyne, G.V., & Dyck, H.M. 1973, *ApJ*, 184, 173
- Cassinelli, J.P., Nordsieck, K.H., & Murison, M.A. 1987, *ApJ*, 317, 290
- Collins, G.W., II, Truax, R.Y., & Cranmer, S.R. 1991, *ApJS*, 77, 541
- Coyne, G.V. & McLean, I.S. 1982, in *IAU Symp. 98: Be Stars*, ed. M. Jaschek & H. Groth, (Dordrecht: Reidel), 77
- Fox, G.K. 1991, *ApJ*, 379, 663
- Hillier, D.J. 1994, *A&A*, 289, 492
- Kruszewski, A., Gehrels, T., & Serkowski, K. 1968, *AJ*, 73, 677
- Kurucz, R.L. 1994, *Solar Model Abundance Model Atmospheres*, Smithsonian Astrophysical Observatory, CD-ROM No. 19
- McDavid, D. 1999, *PASP*, 111, 494
- McLean, I.S. 1979, *MNRAS*, 186, 265
- Millar, C.E. & Marlborough, J.M. 1998, *ApJ*, 494, 715
- Poeckert, R. & Marlborough, J.M. 1978a, *ApJ*, 220, 940
- Poeckert, R. & Marlborough, J.M. 1978b, *ApJS*, 38, 229
- Quirrenbach, A., Bjorkman, K.S., Bjorkman, J.E., Hummel, C.A., Buscher, D.F., Armstrong, J.T., Mozurkewich, D., Elias, N.M., II, & Babler, B.L. 1997, *ApJ*, 479, 477
- Slettebak, A. 1982, *ApJS*, 50, 55
- Waters, L.B.F.M., Coté, J., & Lamers, H.J.G.L.M. 1987, *A&A*, 185, 206
- Waters, L.B.F.M. & Marlborough, J.M. 1992, *A&A*, 256, 195
- Wood, K., Bjorkman, K.S., & Bjorkman, J.E. 1997, *ApJ*, 477, 926